

A Statistical Characterization of Localization Performance in Millimeter-Wave Cellular Networks

Jiajun He, *Student Member, IEEE*, Young Jin Chun, *Member, IEEE*

Abstract—Millimeter-wave (mmWave) communication is a promising solution for achieving high data rate and low latency in 5G wireless cellular networks. Since directional beamforming and antenna arrays are exploited in the mmWave networks, accurate angle-of-arrival (AOA) information can be obtained and utilized for localization purposes. The performance of a localization system is typically assessed by the Cramér-Rao lower bound (CRLB) evaluated based on fixed node locations. However, this strategy only produces a fixed value for the CRLB specific to the scenario of interest. To allow randomly distributed nodes, stochastic geometry has been proposed to study the CRLB for time-of-arrival-based localization. To the best of our knowledge, this methodology has not yet been investigated for AOA-based localization. In this work, we are motivated to consider the mmWave cellular network and derive the CRLB for AOA-based localization and its distribution using stochastic geometry. We analyze how the CRLB is affected by the node locations' spatial distribution, including the target and participating base stations. To apply the CRLB on a network setting with random node locations, we propose an accurate approximation of the CRLB using the $\lceil L/4 \rceil$ -th value of ordered distances where L is the number of participating base stations. Furthermore, we derive the localizability of mmWave network, which is the probability that a target is localizable, and examine how the network parameters influence the localization performance. These findings provide us deep insight into optimum network design that meets specified localization requirements.

Index Terms—Millimeter-wave, angle-of-arrival, localizability, Cramér-Rao lower bound.

I. INTRODUCTION

DUE to the emergence of internet-of-things, positioning techniques have received considerable attention, which can be utilized to enhance user experience of location-based services, including navigation, mapping, and intelligent transportation systems [1]. Fifth-generation (5G) wireless network access interface together with its large bandwidth, high carrier frequency, and massive antenna array offers excellent opportunities for accurate localization, and millimeter-wave (mmWave) is a promising technology for the 5G wireless communication systems to meet such requirements. Wireless networks enable us to obtain accurate location-bearing information from estimating the channel parameters, such as time-of-arrival (TOA), time-difference-of-arrival (TDOA), received signal strength (RSS), and angle-of-arrival (AOA). In mmWave networks, we can exploit the large antenna array

and highly directional transmission to acquire the AOAs with high precision [2]. Large-scale directional antenna arrays are leveraged due to the small wavelength of mmWave signals, which can generate highly directional beams and provide large beamforming gain [3]. In this paper, we analyze the localization performance of the mmWave wireless network using the AOA measurements.

A target is *localizable* if its position can be determined without ambiguity with a sufficient number of participating base stations (BSs). The AOA-based positioning requires at least 2 BSs to determine the location of the target in a two-dimensional (2-D) plane [4]. Since the number of participating BSs determines the accuracy of the localization, we introduce the notion of L -localizability, which indicates the probability of at least L BSs participating in the localization procedure.

Furthermore, Cramér-Rao lower bound (CRLB) is a standard tool to analyze the performance of localization algorithm, which provides a lower bound for the position error of any unbiased estimator [4]. Conventionally, CRLB assumes a fixed scenario, where the nodes are placed at a particular geometry, and this assumption limits the applicability of CRLB as it cannot properly reflect the impact of the random geometry. To evaluate the localization error of a random network, we use stochastic geometry [5], [6] and consider the ensemble average of the node spatial locations. Then the CRLB is no longer a fixed value, but rather a random variable (RV) conditioned on the number of participating BSs, where the randomness of CRLB is induced by the randomness of the nodes. Based on the L -localizability and random CRLB, we provide a deep insight for the network operator on how to deploy the BSs to achieve a given localization requirement. The main contributions of this paper are summarized as follows.

1) *L-Localizability*: We derive the tractable expression of L -localizability to study the number of BSs who can participate in a localization procedure. In [7], the authors studied on how the network parameters affect the localization performance of the Long Term Evolution (LTE) cellular network. In this work, we derive the L -localizability for the mmWave networks, where the impacts of the directional antenna and Nakagami fading on mmWave-based localization systems are assessed. Furthermore, we introduce asymptotic bounds and approximations for the distribution of the L -localizability and CRLB to provide analytical tools to track the performance of localization systems.

2) *Random AOA-based CRLB*: In the mmWave networks, accurate AOA measurements can be obtained by using antenna arrays to locate the target of interest with high precision. In this paper, we derive random CRLB for AOA-based positioning.

This work was supported by in part by the City University of Hong Kong (CityU), Startup Grant 7200618, and in part by the CityU, Strategic Research Grant 21219520

J. He and Y. J. Chun are with the Department of Electrical Engineering, City University of Hong Kong, Hong Kong, China (e-mail: jiajunhe5-c@cityu.edu.hk; yjchun@cityu.edu.hk)

Previous works [8]–[10] applied stochastic geometry to TOA-based localization, and to the best of our knowledge, there is no prior work that investigates random geometry on AOA-based localization systems. We derive the distribution of AOA-positioning based CRLB for the mmWave networks by using stochastic geometry and order statistics. The obtained distribution shows how the network parameters affect localization performance in the mmWave wireless networks.

The rest of this paper is organized as follows. Relevant works are reviewed in Section II, the system model is presented in Section III, and we analyze the localization performance in Section IV. Numerical results are provided in Section V and we conclude the paper in Section VI.

II. RELATED WORK

The major localization techniques in the LTE mobile network are TDOA [11], [12], uplink TDOA [13], measurement report (MR) [14] and enhanced cell ID (E-CID) [15]. Compared with the LTE mobile network, mmWave is regarded as a promising candidate to meet demands for achieving accurate localization in the 5G mobile network. Conventionally, the localization approaches can be divided into two categories: direct and indirect localization. In the mmWave networks, we focus on the latter due to the high computational complexity of the former. The target of interest can be located in mmWave networks using the indirect approach by estimating the channel parameters, including TOA, AOA, and RSS [16]. Based on the processing methods of mmWave signals, localization approaches can be categorized into proximity, fingerprinting, and geometry-based [17]. In this paper, we mainly focus on the geometry-based positioning approach because large-scale antenna arrays can provide high angular resolution [18].

Localization performance is generally evaluated using CRLB for a fixed geometry [4]. For considering all possible localization scenarios, we aim to derive the network-wide distribution of localization performance, and there are two important metrics, namely, the probability that a given number of BSs can participate in a localization procedure, and the distribution of the CRLB conditioned on the number of participating BSs. The first metric, which includes finding the participation probability of a given number of BSs, was studied in [7]. The authors modeled a cellular network with a homogeneous Poisson point process (PPP) [5] and applied a “dominant interferer analysis” to derive an expression for the probability of L -localizability. However, this method is only suitable for LTE mobile networks. Compared with [7], we derive an accurate expression of L -localizability using Alzer’s inequality [19] for characterizing the localization performance of mmWave wireless networks.

Regarding the second metric, there have been several attempts in the literature to achieve this conditional distribution of CRLB. In [20], approximations of this conditional distribution were presented for RSS and TOA localization systems. However, these distributions are sensitive to the number of participating BSs, and it is only accurate for numerous participating BSs. In real-world scenarios, we prefer to measure the conditional distribution using smaller number

of participating BSs because this is more common in cellular networks. Additionally, [8] presented an analysis of how the CRLB is affected by the order statistics of internodal angles. This analysis reveals a connection between the second largest internodal angle and the CRLB, leading to an accurate approximation of the CRLB. However, only TOA-based localization is considered in a general fading channel which takes the large-scale fading into consideration. Motivated by these works, we explore the localization performance using the AOA measurements and apply it in the mmWave-based cellular network. Different from [8], we analyze how the CRLB is affected by the ordered distances between BSs and target, and an accurate approximation of the CRLB is provided using the $[L/4]$ -th distance between these ordered distances, where L is the number of participating BSs in a localization procedure.

III. SYSTEM MODEL

In this section, we describe the system model where the key notations used in this paper are summarized in Table 1.

A. Network Model

We consider downlink transmission in a mmWave cellular network where the locations of BSs are modeled using a homogeneous PPP [5]. As illustrated in Fig. 1, we assume that the target is located at the origin O and the BSs are randomly distributed over the \mathbb{R}^2 plane. The red triangle represents the nearest BS to the target that is located inside the disk, whereas the green triangle indicates the furthest BS from the target residing in the disk. Furthermore, blue and yellow triangles represent the BSs that are located inside and outside the disk, respectively. Let us denote the locations of the BS as $\psi_l = [x_l, y_l] \in \mathbb{R}^2$ and the distance between the l -th BS and target as $r_l = \|\psi_l\|$. Based on the system model, the probability density function (PDF) and cumulative distribution function (CDF) of the L -th nearest BS are given by [21]

$$\begin{aligned} f_{r_L}(r) &= \frac{2(\lambda\pi r^2)^L}{r(L-1)!} e^{-\lambda\pi r^2}, \\ F_{r_L}(r) &= 1 - \sum_{n=0}^{L-1} \frac{1}{n!} e^{-2\pi\lambda r^2} (2\pi\lambda r^2)^n, \end{aligned} \quad (1)$$

where λ represents the BS density. Conditioned on the distance of the L -th BS from O , the remaining BSs closer to the origin than the L -th BS form a uniform binomial point process (BPP) on $\mathbf{b}(O, R_L)$ [22], where the PDF and CDF of r_l are given by

$$f_{r_l}(r) = \frac{2r}{r_L^2 - r_1^2}, \quad F_{r_l}(r) = \frac{r^2}{r_L^2 - r_1^2}, \quad (2)$$

with $r_1 \leq r_l \leq r_L$. In Section IV, we applied order statistic to obtain the distribution of the ordered distances.

B. Channel Model

We assume that each BS is equipped with a directional antenna array composed of N_t elements and all BSs operate at a constant power P_t . In the mmWave channel, the non-line-of-sight (NLOS) interference is negligible since the channel gains of NLOS paths are typically 20 dB weaker than those from

Table I
SUMMARY OF NOTATION

Notation	Meaning
T	transpose
H	conjugate transpose
$\ \cdot\ $	Euclidean norm
ψ_l	location of l -th BS
ψ_t	location of target
r_l	distance between l -th BS and target
r_1	distance between closest BS and target
r_L	distance between furthest BS and target
λ	BS density in the disk
P_t	BS and target transmit power
N_t	number of antenna elements
N	number of clusters
ρ_{ψ_n}	small-scale fading gain
d	antenna spacing
λ_w	antenna wavelength
θ_{ψ}	AOA of BS at location ψ
$n_{AOA,l}$	WGN with zero mean and variance of $\sigma_{AOA,l}^2$
G_1	main-lobe gain
G_2	side-lobe gain
p_a	probability of main-lobe gain is received
p_b	probability of side-lobe gain is received
P_T	total transmit power
P_m	power spectrum density of main-lobe
P_s	power spectrum density of side-lobe
σ_n^2	normalized noise power
a_i	network load indicator
q	probability of BS is activated
α	path-loss exponent
Ω	total number of activated BSs
τ	signal-to-interference-plus-noise ratio threshold
γ	maximum number of selectable BSs
σ_{AOA}	standard deviation of AOA measurement
G_c	average channel gain of mmWave network
N_0	spectral density of WGN
W_{TOT}	total mmWave system bandwidth

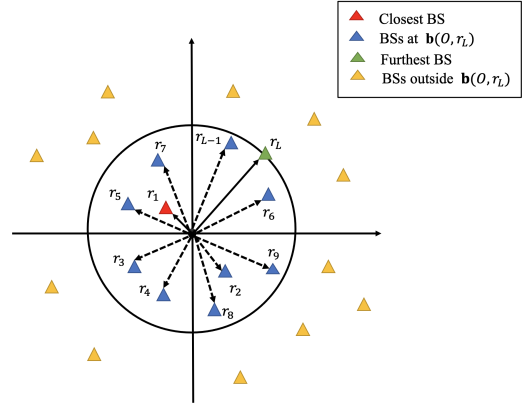


Fig. 1. System model of the mmWave wireless networks

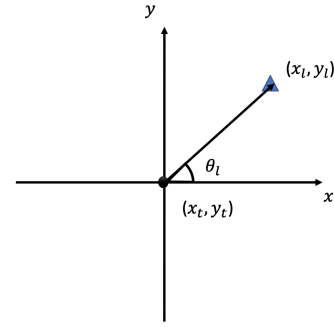


Fig. 2. AOA-based positioning

the line-of-sight (LOS) [23]. The effect of path-loss can be reduced due to the utilization of the directional antenna arrays, and it is also applied to provide highly directional beams. The received signal from the l -th BS to the origin is given by

$$y(t) = \sqrt{P_t} \beta \mathbf{h}_{\psi_l} \mathbf{w}_{\psi_l} r_l^{-\frac{\alpha}{2}} s_{\psi_l}(t) + n(t) + \sum_{\psi \in \psi'} \sqrt{P_t} \beta \mathbf{h}_{\psi} \mathbf{w}_{\psi} \|\psi\|^{-\frac{\alpha}{2}} s_{\psi}(t), \quad t \in [0, T], \quad (3)$$

where $s_{\psi}(t)$ is the transmit signal, \mathbf{h}_{ψ} is the channel vector, α and β respectively represent the path-loss exponent and path-loss intercept, \mathbf{w}_{ψ} denotes the beamforming vector of the node at location ψ , and $n(t)$ represents the additive white Gaussian noise (AWGN) with variance σ^2 . Note that the locations of the interfering transmitters are denoted as ψ' .

Due to high free-space path-loss, the mmWave propagation environment is well characterized by a clustered channel model, known as the Saleh-Valenzuela model [24]:

$$\mathbf{h}_{\psi} = \sqrt{N_t} \sum_{n=1}^N \rho_{\psi,n} \mathbf{a}_t^H(\theta_{\psi,n}), \quad (4)$$

where N is the number of clusters and $\rho_{\psi,n}$ represents the complex small-scale fading coefficient of the n -th cluster. We assume that the fading channel power gain follows a gamma distribution, i.e., $|\rho_{\psi}|^2 \sim \Gamma(M, \frac{1}{M})$, with Nakagami parameter M . In this paper, we focus on LOS paths, i.e., $N = 1$,

and adopt a uniformly random single path (UR-SP) channel model that is commonly used in the mmWave network analysis [25]. The $\mathbf{a}_t(\theta_{\psi})$ represents the transmit array response vector corresponding to the AOA θ_{ψ} . We consider a uniform linear array (ULA) with N_t antenna elements, where the transmit array response vectors are given by

$$\mathbf{a}_t(\theta_{\psi}) = \frac{1}{\sqrt{N_t}} \left[1, \dots, e^{j2\pi k \theta_{\psi}}, \dots, e^{j2\pi(N_t-1)\theta_{\psi}} \right]^T, \quad (5)$$

where d is the antenna spacing, λ_w represents the wavelength, ϕ_{ψ} denotes the AOA, $k \in [0, N_t]$ is the antenna index, and $\theta_{\psi} = \frac{d}{\lambda_w} \sin \phi_{\psi}$ is uniformly distributed over $\left[-\frac{d}{\lambda_w}, \frac{d}{\lambda_w}\right]$.

Once the AOA measurements are obtained, we compute the location of the target, where we assume LOS propagation. As shown in Fig. 2, we denote the AOA between the target and l -th BS as θ_l and the location of target as $\psi_t = [x_t, y_t]$,

$$\tan(\theta_l) = \frac{y_l - y_t}{x_l - x_t}, \quad l = \{1, \dots, L\}. \quad (6)$$

The AOA measurement at the l -th BS is modeled as follows

$$r_{AOA,l} = \theta_l + n_{AOA,l} = \tan^{-1} \left(\frac{y_l - y_t}{x_l - x_t} \right) + n_{AOA,l}, \quad (7)$$

where $n_{AOA,l}$ is the AWGN with variance $\sigma_{AOA,l}^2$. The AOA measurements in (7) can be represented by a vector form

$$\mathbf{r}_{AOA} = \mathbf{f}_{AOA}(\psi) + \mathbf{n}_{AOA,l}, \quad (8)$$

where \mathbf{r}_{AOA} , \mathbf{n}_{AOA} , and $\mathbf{f}_{\text{AOA}}(\boldsymbol{\psi})$ are respectively defined by

$$\begin{aligned} \mathbf{r}_{\text{AOA}} &= [r_{\text{AOA},1}, r_{\text{AOA},2}, \dots, r_{\text{AOA},L}]^T, \\ \mathbf{n}_{\text{AOA}} &= [n_{\text{AOA},1}, n_{\text{AOA},2}, \dots, n_{\text{AOA},L}]^T, \\ \mathbf{f}_{\text{AOA}}(\boldsymbol{\psi}) &= \left[\tan^{-1} \left(\frac{y_1 - y_t}{x_1 - x_t} \right), \dots, \tan^{-1} \left(\frac{y_L - y_t}{x_L - x_t} \right) \right]^T. \end{aligned} \quad (9)$$

C. Analog Beamforming and Antenna Radiation Pattern

Assuming that the AOA of the channel between the BS at location $\boldsymbol{\psi}_l$ and its serving user at location $\boldsymbol{\psi}_t$ is θ_{ψ_l} , the beamforming vector is given by

$$\mathbf{w}_{\psi_l} = \mathbf{a}_t(\theta_{\psi_l}), \quad (10)$$

which means that the BS should align the beam direction exactly with the propagation channel to obtain the maximum power gain. However, the beam direction cannot always align with the transmit signal. Hence, we consider the single main-lobe and single side-lobe at antennas of both BS and mobile user, and all lobes are approximated by a flat-top antenna pattern [26]. That is, the single main-lobe with beam-width θ_1 has antenna gain G_1 and each side lobe with identical beam-width θ_2 has antenna gain G_2 . We assume that the power spectrum density (PSD) of the main-lobe and side-lobe at a distance r are denoted as P_m and P_s . Hence, the total transmit power P_T consists of the main-lobe and side-lobe radiation powers, which is given by [26]

$$P_T = P_m 2\pi r^2 \left[1 - \cos \frac{\theta_1}{2} \right] + N_t P_s 2\pi r^2 \left[1 - \cos \frac{\theta_2}{2} \right], \quad (11)$$

where $P_m = G_1 P_T / 4\pi r^2$ and $P_s = G_2 P_T / 4\pi r^2$. Let us denote $k = G_2 / G_1$ where $k \in (0, 1)$, i.e., $G_2 = kG_1$.

For the associated signal transmission, we assume perfect alignment where both the BS and user utilize the main-lobe, achieving the squared gain G_1^2 . For the interfering signal, the interfering BSs are randomly distributed in $[0, 2\pi)$. The transmit antenna gain G_{Tx} at the transmitter and the receive antenna gain G_{Rx} at the receiver are randomly chosen from a discrete set $\{G_1, G_2\}$ with probability $p_a = \frac{\theta_1}{2\pi}$ and $p_b = 1 - p_a$, respectively. Let $G_{TRx} = G_{Tx} G_{Rx}$, we have

$$G_{TRx} = \begin{cases} G_1^2, & p_1 = p_a^2 \\ G_1 G_2, & p_2 = 2p_a p_b \\ G_2^2, & p_3 = p_b^2. \end{cases} \quad (12)$$

Based on the antenna radiation pattern, the product of small-scale fading gain and beamforming gain of the BS at location $\boldsymbol{\psi}$ is computed as:

$$|\mathbf{h}_{\boldsymbol{\psi}} \mathbf{w}_{\boldsymbol{\psi}}|^2 = N_t |\rho_{\boldsymbol{\psi}}|^2 G_{TRx}. \quad (13)$$

IV. PERFORMANCE ANALYSIS

In this section, we analyze the performance of AOA-based localization over a mmWave network. To evaluate the localization performance, we will introduce two metrics; L -localizability and AOA-based random CRLB.

A. L -Localizability

A target is *localizable* if there are a sufficient number of participating BSs such that the localization procedure can be conducted. We introduce L -Localizability, which is a probability to have L localizable BSs within the network [7]. Conventionally, commonly-accepted minimum values of L for the unambiguous operation of a localization system are 2, 3, 3 and 3 for AOA, TOA or RSS, and TDOA, respectively [4]. If we treat the interference originated from outside of the circular disk with radius R_L as a noise, the signal-to-interference-plus-noise ratio (SINR) of the link from the k -th BSs to the target can be expressed as a function of L as

$$\text{SINR}_k(L) = \frac{G_1^2 |\rho_{\boldsymbol{\psi}_k}|^2 r_k^{-\alpha}}{\sigma_n^2 + J}, \quad (14)$$

where $\sigma_n^2 = \frac{\sigma_T^2 + \sigma_{\text{out}}^2}{\beta P_t N_t}$ is the normalized noise power, including the thermal noise power σ_T^2 and interference power σ_{out}^2 outside the circular disk. The interference from nodes inside the disk, denoted by J , is expressed as:

$$J = \sum_{i=1, i \neq k}^{L-1} a_i G_{TRx,i} |\rho_{\boldsymbol{\psi}_i}|^2 \|\boldsymbol{\psi}_i\|^{-\alpha}, \quad (15)$$

where $a_i \in \{0, 1\}$ is utilized to simulate the network load. The probability of $a_i = 1$ equals q which is the probability of a BS inside the disk to be activated. The a_i represents whether the BS is activated in the localization procedure and we assume that the activation probability $P(a_i = 1) = q$ is fixed throughout the localization procedure.

For a given $\boldsymbol{\psi} \in \mathbb{R}^2$, a mobile device is said to be L -localizable if at least L BSs participate in the localization procedure. Let us denote the SINR threshold as τ and the maximum number of BSs that can participate in the localization procedure as γ , defined as

$$\gamma = \arg \max_L \left(L \cdot \prod_{k=1}^L \mathbb{I}(\text{SINR}_k(l) \geq \tau) \right), \quad (16)$$

where $\mathbb{I}(\cdot)$ is the indicator function. Then, the L -localizability, denoted by P_L , is derived as:

$$P_L = P(\gamma \geq L) = \mathbb{E} \left[\prod_{k=1}^L \mathbb{I}(\text{SINR}_k(l) \geq \tau) \right]. \quad (17)$$

Since the SINR from a BS farther from the mobile device is lower than that of the closer BS, the following inequality holds: $\mathbb{I}(\text{SINR}_k(L) \geq \tau) \geq \mathbb{I}(\text{SINR}_l(L) \geq \tau)$ for all $k \geq l \geq$

L . Then, the L -localizability P_L can be computed as follows

$$\begin{aligned}
P_L &= \mathbb{E} [\mathbb{I}(\text{SINR}_L(L) \geq \tau)] = P(\text{SINR}_L(L) \geq \tau) \\
&= 1 - P\left(|\rho_{\psi_L}|^2 \leq \frac{\tau r_L^\alpha}{G_1^2} (\sigma_n^2 + J)\right) \\
&\stackrel{a}{\approx} 1 - \mathbb{E}_{r_L} \left[\left(1 - e^{-\nu \frac{\tau}{G_1^2} r_L^\alpha (\sigma_n^2 + J)}\right)^M \right] \\
&\stackrel{b}{=} \mathbb{E}_{r_L} \left[\sum_{i=1}^M (-1)^{i+1} \binom{M}{i} e^{-s \sigma_n^2} \mathcal{L}_I(s) \right] \\
&= \int_0^\infty f_{r_L}(r) \sum_{i=1}^M (-1)^{i+1} \binom{M}{i} e^{-s \sigma_n^2} \mathcal{L}_I(s) dr
\end{aligned} \tag{18}$$

where $\nu = M(M!)^{-\frac{1}{M}}$, $s = i\nu \frac{\tau}{G_1^2} r_L^\alpha$ and $\mathcal{L}_I(s) = \mathbb{E}_I[e^{-sJ}]$ is the Laplace transform of the interference. Step (a) follows by the Alzer's inequality and (b) is obtained based on the binomial expansion. The Laplace transform of the interference is [27]

$$\begin{aligned}
\mathcal{L}_I(s) &= \mathbb{E}_I[e^{-sJ}] \\
&= \exp \left[-2\pi\lambda q \underbrace{\int_{r_1}^{r_L} (1 - \mathbb{E}_{g_\psi}[e^{-sJ}]) r dr}_{\triangleq \Lambda} \right], \tag{19}
\end{aligned}$$

where $g_\psi = G_{TRx} |\rho_\psi|^2$ represents the combined effect of antenna gain and channel gain at the location ψ . The term Λ is computed as:

$$\begin{aligned}
\Lambda &= \int_{r_1}^{r_L} (1 - \mathbb{E}_{g_\psi}[e^{-sJ}]) r dr \\
&= -\frac{1}{2} \left[r_L^2 - \delta r_L^2 \mathbb{E}_{g_\psi} [E_{1+\delta}(s g_\psi r_L^{-\alpha})] \right. \\
&\quad \left. - r_1^2 + \delta r_1^2 \mathbb{E}_{g_\psi} [E_{1+\delta}(s g_\psi r_1^{-\alpha})] \right], \tag{20}
\end{aligned}$$

where $\delta = \frac{2}{\alpha}$ and $E_{1+\delta}(\cdot)$ is the generalized exponential integral [28]. The term $\mathbb{E}_{g_\psi} [E_{1+\delta}(s g_\psi r^{-\alpha})]$ is given by

$$\begin{aligned}
&\mathbb{E}_{g_\psi} [E_{1+\delta}(s g_\psi r^{-\alpha})] \\
&= \frac{s^\delta \Gamma(-\delta)}{r^2} \left[\mathbb{E}_{g_\psi} [g_\psi^\delta] + \frac{\alpha}{2} - \sum_{p=1}^{\infty} \frac{(-s)^p \cdot \mathbb{E}_{g_\psi} [g_\psi^\delta]}{r^{\alpha p} \cdot p! \cdot (p - \delta)} \right], \tag{21}
\end{aligned}$$

and the fractional moment of g_ψ is derived as:

$$\begin{aligned}
\mathbb{E}_{g_\psi} [g_\psi^\delta] &= \mathbb{E}_{|\rho_\psi|^2, G_{TRx}} \left[(|\rho_\psi|^2 G_{TRx})^\delta \right] \\
&= \frac{\Gamma(M + \delta)}{\Gamma(M) M^\delta} \cdot \mathbb{E}_{G_{TRx}} (G_{TRx}^\delta) \\
&= \frac{\Gamma(M + \delta)}{\Gamma(M) M^\delta} \cdot [G_1^{2\delta} p_a^2 + 2(G_1 G_2)^\delta p_a p_b + G_2^{2\delta} p_b^2]. \tag{22}
\end{aligned}$$

Hence, the L -localizability can be numerically evaluated by substituting (19)-(22) into (18).

B. Approximation of Cramér-Rao Lower Bound

We derive the AOA-based random CRLB using the Fisher information matrix (FIM), denoted by $\mathbf{I}(\psi)$ [4]

$$\mathbf{I}(\psi) = \left(\frac{\partial \mathbf{f}_{\text{AOA}}(\psi)}{\partial \psi} \right)^T \mathbf{C}_{\text{AOA}}^{-1} \frac{\partial \mathbf{f}_{\text{AOA}}(\psi)}{\partial \psi}, \tag{23}$$

where $\mathbf{C}_{\text{AOA}}^{-1}$ represents the inverse of the noise covariance matrix and the derivative of $\mathbf{f}_{\text{AOA}}(\psi)$ which is the angle vector with respect to ψ are given by

$$\begin{aligned}
\mathbf{C}_{\text{AOA}}^{-1} &= \text{diag} \left(\frac{1}{\sigma_{\text{AOA},1}^2}, \frac{1}{\sigma_{\text{AOA},2}^2}, \dots, \frac{1}{\sigma_{\text{AOA},L}^2} \right), \\
\frac{\partial \mathbf{f}_{\text{AOA}}(\psi)}{\partial \psi} &= - \begin{bmatrix} \frac{y-y_1}{(x-x_1)^2+(y-y_1)^2} & \frac{x-x_1}{(x-x_1)^2+(y-y_1)^2} \\ \frac{y-y_2}{(x-x_2)^2+(y-y_2)^2} & \frac{x-x_2}{(x-x_2)^2+(y-y_2)^2} \\ \vdots & \vdots \\ \frac{y-y_L}{(x-x_L)^2+(y-y_L)^2} & \frac{x-x_L}{(x-x_L)^2+(y-y_L)^2} \end{bmatrix}. \tag{24}
\end{aligned}$$

Without loss of generality, σ_{AOA} is considered to be a known quantity and assumed to be identical for each BSs, *i.e.*, $\sigma_{\text{AOA},1} = \sigma_{\text{AOA},2} = \dots = \sigma_{\text{AOA},L}$ [8]. The numerical value of σ_{AOA} depends on the average SNR of the mmWave networks, denoted by $\overline{\text{SNR}}$, as follows

$$\overline{\text{SNR}} = \frac{G_c P_t}{N_0 W_{\text{TOT}}} \tag{25}$$

where G_c is the average channel gain, N_0 is the spectral density of the WGN, and W_{TOT} is the total system bandwidth [29], [30]. Hence, $\mathbf{I}(\psi)$ is

$$\begin{aligned}
&\mathbf{I}_{\text{AOA}}(\psi) \\
&= \sigma_{\text{AOA}}^2 \begin{bmatrix} \sum_{i=1}^L \frac{(y-y_i)^2}{r_i^4} & -\sum_{i=1}^L \frac{(x-x_i)(y-y_i)}{r_i^4} \\ -\sum_{i=1}^L \frac{(x-x_i)(y-y_i)}{r_i^4} & \sum_{i=1}^L \frac{(x-x_i)^2}{r_i^4} \end{bmatrix}. \tag{26}
\end{aligned}$$

To assess the distribution of the CRLB, we introduce the position error bound (PEB), which is the square root of the CRLB [31]. We will denote the PEB by S and its closed-form expression can be obtained by using (26)

$$S \triangleq \sqrt{\text{CRLB}} = \sqrt{\text{tr}(\mathbf{I}_{\text{AOA}}^{-1}(\psi))} = \sigma_{\text{AOA}} \frac{\sqrt{L}}{\sqrt{Q_1 - Q_2}}, \tag{27}$$

where Q_1 and Q_2 are

$$\begin{aligned}
Q_1 &= \sum_{i=1}^L \frac{(y_i - y_t)^2}{r_i^4} \sum_{j=1}^L \frac{(x_j - x_t)^2}{r_j^4}, \\
Q_2 &= \sum_{i=1}^L \frac{(x_i - x_t)^2 (y_i - y_t)^2}{r_i^8}. \tag{28}
\end{aligned}$$

Since (27) and (28) are functions of $2L$ random variables, *i.e.*, (x_i, y_i) for $1 \leq i \leq L$, we need to simplify (28) using its asymptotic bounds, which will enable us to characterize the distribution of (27). In the following proposition, we derived a tight upper bound for $Q_1 - Q_2$ and through simulation, we verified that approximation error is less than 5% for $L \geq 8$.

Proposition 1. *The random variable $Q_1 - Q_2$ from (27) can be upper bounded as follows*

$$Q_1 - Q_2 \leq \frac{1}{4} \left[\left(\sum_{i=1}^L \frac{1}{r_i^2} \right)^2 - \sum_{i=1}^L \frac{1}{r_i^4} \right] \tag{29}$$

Proof. First, we derive the lower bound of Q_2 as follows

$$Q_2 \stackrel{(a)}{\geq} \sum_{i=1}^L \frac{\frac{1}{4} [(x_i - x_t)^2 + (y_i - y_t)^2]}{r_i^8} \stackrel{(b)}{=} \sum_{i=1}^L \frac{1}{4r_i^4}, \tag{30}$$

where the inequality $(x_i - x_t)^2 + (y_i - y_t)^2 \geq 2(x_i - x_t)(y_i - y_t)$ is applied to step (a) and Cartesian coordinates is converted to polar coordinate in step (b). As shown in Fig. 2, the polar coordinate of (x_i, y_i) is given by

$$x_i - x_t = r_i \cos(\theta_i), \quad y_i - y_t = r_i \sin(\theta_i). \quad (31)$$

Next, we derive the upper bound of Q_1

$$\begin{aligned} Q_1 &= \sum_{i=1}^L \frac{(y_i - y_t)^2}{r_i^4} \sum_{j=1}^L \frac{(x_j - x_t)^2}{r_j^4} \\ &= \sum_{i=1}^L \frac{\sin^2(\theta_i)}{r_i^2} \sum_{j=1}^L \frac{\cos^2(\theta_j)}{r_j^2}, \end{aligned} \quad (32)$$

where we will maximize Q_1 with respect to the phase $\{\theta_i\}$ for a given distance $\{r_i\}$. Then, (32) can be expressed as

$$Q_1 = \sum_{i=1}^L \frac{\sin^2(\theta_i)}{r_i^2} \sum_{j=1}^L \frac{1 - \sin^2(\theta_j)}{r_j} = \xi \left(\sum_{j=1}^L \frac{1}{r_j^2} - \xi \right), \quad (33)$$

where we denote $\xi \triangleq \sum_{i=1}^L \frac{\sin^2(\theta_i)}{r_i^2}$. The first order derivative of Q_1 is zero when $\xi^* = \frac{1}{2} \sum_{i=1}^L \frac{1}{r_i^2}$ and the second order derivative of Q_1 has a negative value at ξ^* as follows

$$\begin{aligned} \frac{\partial Q_1}{\partial \xi} &= \sum_{i=1}^L \frac{1}{r_i^2} - 2\xi = 0 \Rightarrow \xi^* = \frac{1}{2} \sum_{i=1}^L \frac{1}{r_i^2}, \\ \frac{\partial^2 Q_1}{\partial \xi^2} &= -2 < 0. \end{aligned} \quad (34)$$

Hence, the upper bound of Q_1 is given by

$$Q_1 \leq \max_{\{\theta_i\}} Q_1 \Big|_{\xi=\xi^*} = \left(\frac{1}{2} \sum_{i=1}^L \frac{1}{r_i^2} \right)^2. \quad (35)$$

We obtain (29) by (30) and (35). This completes the proof. ■

Based on Proposition 1, the PEB S is lower bounded by

$$S \geq \frac{2\sigma_{\text{AOA}} \cdot \sqrt{L}}{\sqrt{\left(\sum_{i=1}^L \frac{1}{r_i^2}\right)^2 - \sum_{i=1}^L \frac{1}{r_i^4}}} = \frac{2\sigma_{\text{AOA}} \cdot \sqrt{L}}{\sqrt{\sum_{\substack{i,j=1 \\ i \neq j}}^L \frac{1}{r_i^2 r_j^2}}}. \quad (36)$$

In the following assumption, we introduced an approximation of (36), which provides a tractable asymptotic bound of S . Through simulation, we justified the approximation accuracy.

Assumption 1. Assume that the link distances are sorted in an ascending order, i.e., $R = [r_1, \dots, r_L]$ and $r_1 \leq r_2 \leq \dots \leq r_L$. The denominator of (36) can be approximated as follows

$$D \triangleq \sum_{\substack{i,j=1 \\ i \neq j}}^L \frac{1}{r_i^2 r_j^2} \approx \frac{L(L-1)}{r_{\lceil L/4 \rceil}^4}, \quad (37)$$

where $r_{\lceil L/4 \rceil}$ is the $\lceil L/4 \rceil$ -th link distance in the ordered set $R = [r_1, \dots, r_L]$ and L is the number of participating BSs.

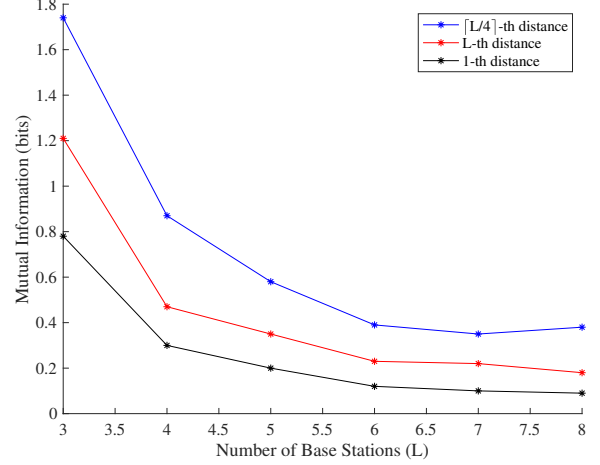


Fig. 3. Impact of distance selection on mutual information

Remark 1. We validated (37) through simulation, where we repeated the realization of the anchor nodes 10 million times. Since the set R is sorted, the term D in (37) is bounded by

$$\frac{L(L-1)}{r_L^4} \leq \sum_{\substack{i,j=1 \\ i \neq j}}^L \frac{1}{r_i^2 r_j^2} \leq \frac{L(L-1)}{r_1^4}. \quad (38)$$

We attempt to find the k -th term r_k in set R that provides the most accurate approximation to D . To solve this problem, we used heuristic approach and evaluated the mutual information between D and the random variable r_k for a given L as follows

$$\min_{1 \leq k \leq L} \mathbb{E} \left[\left| D - \frac{L(L-1)}{r_k^4} \right|^2 \right] \Leftrightarrow \max_{1 \leq k \leq L} I(D; r_k | L = l), \quad (39)$$

where the mutual information conditioned on L is defined as

$$I(D; r_k | L = l) = h(D | L = l) - h(D | r_k, L = l), \quad (40)$$

and the differential entropies are given by

$$\begin{aligned} h(D | L = l) &= - \sum_{d \in D} f_D(d|l) \log_2 f_D(d|l), \\ h(D | r_k, L = l) &= - \sum_{\substack{d \in D \\ r_k \in R_k}} f_{D;r_k}(d|r, l) \log_2 f_{D;r_k}(d|r, l), \end{aligned} \quad (41)$$

where R_k and D are the supports of r_k and d , respectively [32]. This approach, which was motivated by [33], can search for the r_l that contains the most information of D . Through an extensive simulation across a range of L , we observed that the $\lceil L/4 \rceil$ -th distance maximizes the mutual information as illustrated in Fig. 3, which justifies Assumption 1, and thus we can use the $\lceil L/4 \rceil$ -th distance to approximate D .

Based on (36) and (37), we can approximate S by

$$S \approx \frac{2\sigma_{\text{AOA}}}{\sqrt{L-1}} r_{\lceil L/4 \rceil}^2, \quad (42)$$

where S is a function of $r_{\lceil L/4 \rceil}$. In the following proposition, we derived the distribution of S using order statistic.

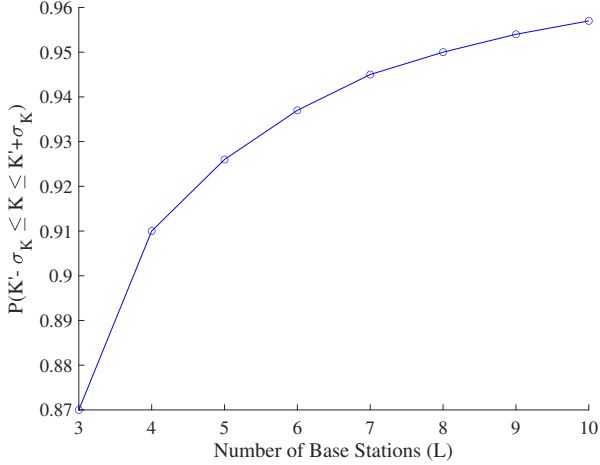


Fig. 4. Probability of $K' - \sigma_K \leq K \leq K' + \sigma_K$

Proposition 2. Assume that the number of participating BSs L , the variance of the range error σ_{AOA} , and the link distance to the closest node r_1 and furthest node r_L are known. Then, the CDF of PEB S is given by

$$F_S(s|L, \sigma_{\text{AOA}}) = F_{r_{\lfloor L/4 \rfloor}} \left[\sqrt{\frac{s}{2} \cdot \frac{\sqrt{L-1}}{\sigma_{\text{AOA}}}} \middle| L, \sigma_{\text{AOA}} \right], \quad (43)$$

where $F_{r_n}(r)$ is the CDF of the n -th order statistic.

Proof. First, the PDF of the n -th order statistic $f_{r_n}(r)$ is [34]

$$f_{r_n}(r) = L f_n(r) \binom{L-1}{n-1} F_{r_n}(r)^{n-1} (1 - F_{r_n}(r))^{L-n}, \quad (44)$$

where $f_n(r)$ and $F_{r_n}(r)$ are given in (2). The CDF $F_{r_n}(r)$ can be derived by integrating (44) as follows

$$\begin{aligned} F_{r_n}(r) &= \int_0^r f_{r_n}(r) dr \\ &= \sum_{j=n}^L \binom{L}{j} F_{r_n}(r)^j (1 - F_{r_n}(r))^{L-j} \\ &= \sum_{j=n}^L \binom{L}{j} \left(\frac{r^2}{r_L^2 - r_1^2} \right)^j \left(1 - \frac{r^2}{r_L^2 - r_1^2} \right)^{L-j}. \end{aligned} \quad (45)$$

Hence, the CDF of S , denoted by $F_S(s|L, \sigma_{\text{AOA}}) = P[S \leq s|L, \sigma_{\text{AOA}}]$ is readily computed as

$$F_S(s|L, \sigma_{\text{AOA}}) = P \left[r_n \leq \sqrt{\frac{s}{2} \frac{\sqrt{L-1}}{\sigma_{\text{AOA}}}} \middle| L, \sigma_{\text{AOA}} \right], \quad (46)$$

where the PDF of S can be computed by differentiating (46). This completes the proof. ■

Remark 2. We evaluated the approximation accuracy of (36) and (42) through Monte Carlo simulation. Let us denote

$$K = \sum_{i=1}^L \frac{\sin^2 \theta_i}{r_i^2} \sum_{j=1}^L \frac{\cos^2 \theta_j}{r_j^2}, \quad K' = \frac{1}{4} \left(\sum_{i=1}^L \frac{1}{r_i^2} \right)^2, \quad (47)$$

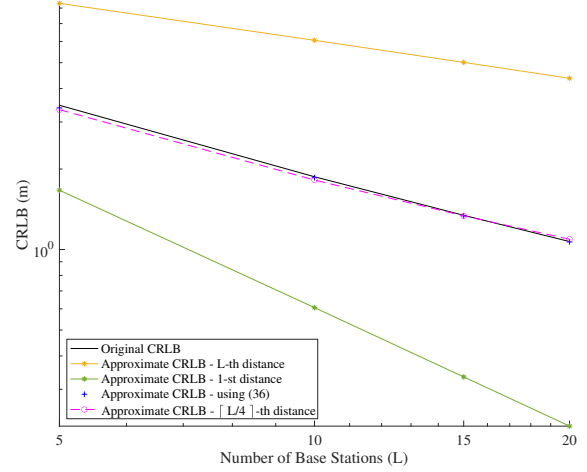


Fig. 5. Original CRLB compared with approximate CRLB

where K is equal to Q_1 in proposition 1 and K' represents the upper bound of Q_1 in (35). We utilized Monte Carlo simulation of 10 million realizations to compute the empirical distribution of K and determine the value of $P[K' - \sigma_K \leq K \leq K' + \sigma_K]$, where the σ_K is the standard deviation of K . Fig. 4 shows the probability $P[K' - \sigma_K \leq K \leq K' + \sigma_K]$ versus a range of L . It is observed that K' can approximate Q with high accuracy. For $L \geq 10$, the approximation accuracy is above 96%.

Furthermore, we compared the CRLB computed by using (27), (36), (42), the 1-st and the L -th ordered distance in Fig. 5. It is observed that the approximations of CRLB using the L -th and 1-st distances cannot approach the original CRLB. However, the asymptotic bound using (36) and the approximation based on (42) closely match the original CRLB curve, which justifies Proposition 1 and Assumption 1.

V. SIMULATION RESULTS

In this section, we evaluate the L -localizability and random AOA-based CRLB for mmWave networks, compare the simulation results to numerical results, and investigate the effect of network parameters on the localization performance. We used MATLAB to randomly simulate a realization of the node deployment 1×10^6 times. It is assumed that the BSs are randomly distributed by a homogeneous PPP with node density $\lambda = 2/\sqrt{3} \times 500^2 \text{m}^2$, bandwidth $W_{\text{TOT}} = 1$ GHz, transmit power $P_T = 1$ Watt, antenna spacing $d = \lambda_w/4$, path-loss intercept $\beta = (\lambda_w/4\pi)^2$, and main-lobe gain $G_1 = 1$ and side-lobe gain $G_2 = 0.2$ with its associate probability $p_a = 0.4$ and $p_b = 0.6$, respectively. Since the NLOS interference is ignored in our model, we choose a σ_{AOA} that accounts for an angular spread under NLOS conditions during simulation.

A. L -localizability Analysis

In Figs. 6-8, we investigate how the network parameters, including network loads, path-loss exponent and Nakagami fading parameter, affect the performance of L -localizability. Fig. 6 compares the L -localizability P_L versus the SINR

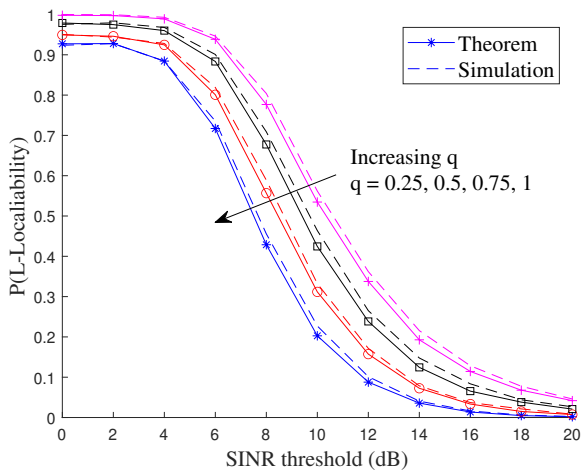


Fig. 6. Impact of the network load on L -localizability when $\alpha = 4$, $N_t = 64$ and $M = 5$

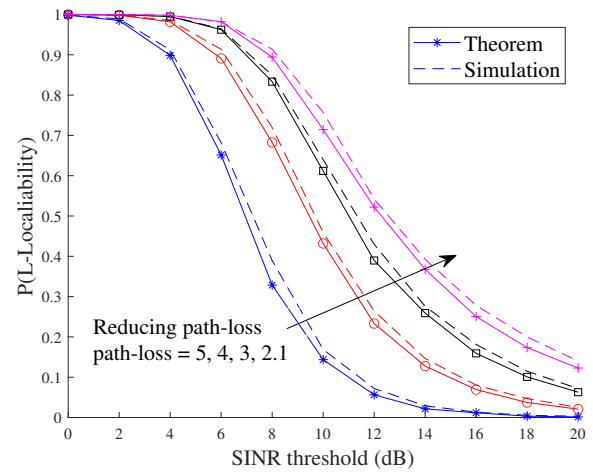


Fig. 7. Impact of path-loss on L -localizability when $\alpha = 4$, $N_t = 64$ and $q = 0.75$

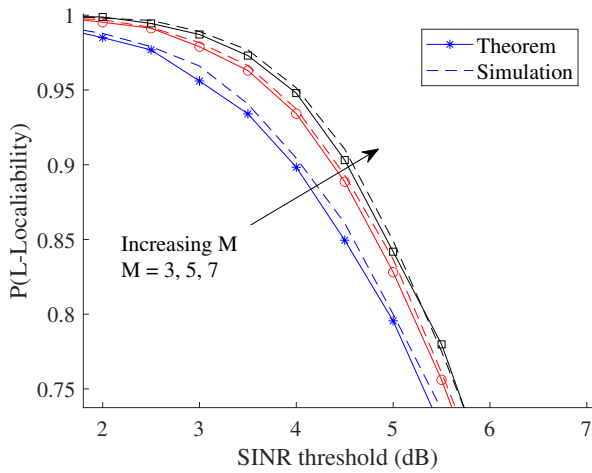


Fig. 8. Impact of Nakagami fading parameter on L -localizability when $\alpha = 2.1$, $N_t = 64$ and $q = 0.75$

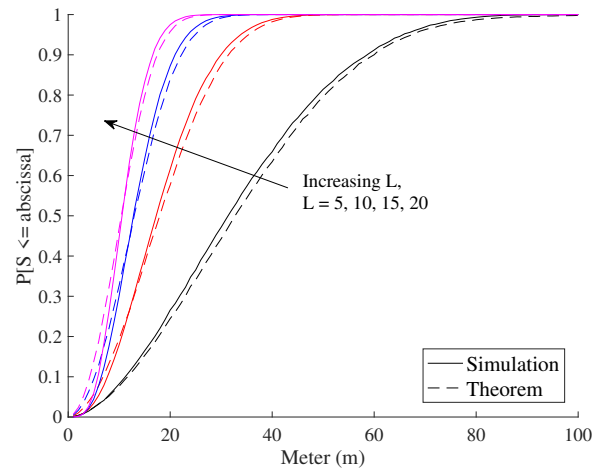


Fig. 9. Impact of number of BSs on the distribution of S when $\alpha = 2$, $N_t = 64$, $M = 5$ and $q = 0.75$

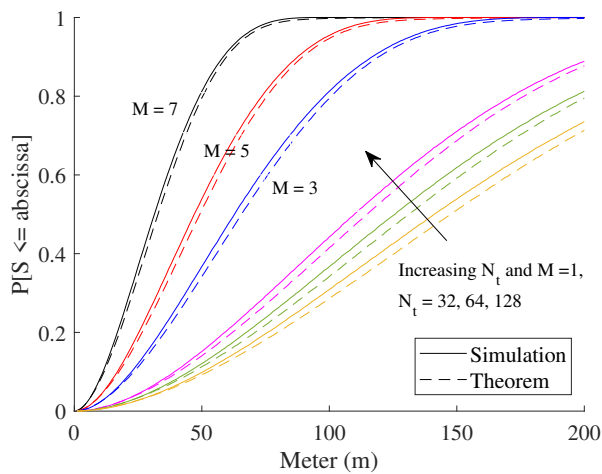


Fig. 10. Impact of M ($M = 3, 5, 7$) on the distribution of S when $\alpha = 2$, $N_t = 64$, $L = 5$, $q = 0.75$ and the impact of N_t ($N_t = 32, 64, 128$) when $\alpha = 2$, $M = 1$, $L = 5$ and $q = 0.75$

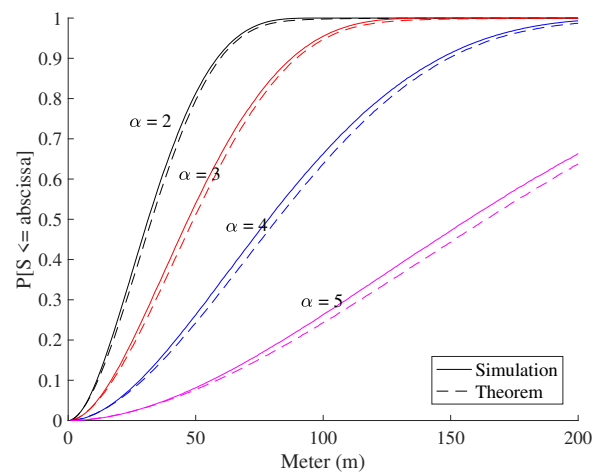


Fig. 11. Impact of path-loss on the distribution of S when $L = 5$, $N_t = 64$, $M = 5$ and $q = 0.75$

threshold for different network loads q . The simulation results are plotted in dotted curves, where as the analytical results are represented by solid curves with a marker. All of the numerical results indicate that the analytical results accurately match the simulation results, justifying the analytical derivation. We observed that increasing the network load leads to a decrease in P_L . It means that network design should be optimized so that there is a sufficient number of BSs to meet the localization requirement. Fig. 7 demonstrates the impact of path-loss on the L -localizability. As the path-loss exponent increases, the transmitted power across the mmWave link will significantly decline, causing a significant drop in P_L . In Fig. 8, we observe the impact of Nakagami fading parameter M on P_L . Since the Nakagami channel becomes deterministic as the M parameter increases, the L -localizability escalates with higher M values.

B. Random AOA-based CRLB Analysis

In Figs. 9-11, we evaluate the distribution of S for various network parameter configurations. Since the approximation of CRLB using $r_{[L/4]}$ provides an accurate approximation to the original CRLB, we used the approximation based on the $[L/4]$ -th distance across Figs. 9-11. In Fig. 9, we examine the impact of the number of participating BSs L on the distribution of S . This is accomplished by varying the number of activated BSs transmitting during a localization procedure. It is observed that the value of $P[S \leq \text{abscissa}]$ increases for a larger L . Since the localization error reduces as the number of BSs increases, a network designer looking to improve the localization accuracy may aim to optimize the network environment to ensure a sufficient number of BSs participate in the localization procedure.

Fig. 10 compares the localization performance for various Nakagami fading parameter M and the number of antenna elements N_t . It is observed that increasing M parameter escalates $P[S \leq \text{abscissa}]$, which improves the localization performance. Furthermore, we demonstrate how the number of antenna elements N_t affects the localization performance. As the number of antenna elements increases, the normalized noise power $\sigma_n^2 = \frac{\sigma_i^2 + \sigma_{\text{out}}^2}{\beta P_t N_t}$ will be reduced, which leads to an increase of $P[S \leq \text{abscissa}]$. This indicates that the localization performance can be enhanced by adding more antenna elements in the BSs, which raises the implementation cost for each BS. Hence, the network designer should find an optimum trade-off between choosing a suitable number of antennas in the BS and enhancing the localization performance. Fig. 11 shows the impact of path-loss on the performance of the mmWave-based localization systems. As the path-loss exponent increases, the value of $P[S \leq \text{abscissa}]$ decline, which is a similar pattern to Fig. 7.

VI. CONCLUSION

This paper presents L -localizability and random AOA-based CRLB for mmWave wireless network, where we used stochastic geometry to account for all possible positioning scenarios. We derived the L -localizability and random CRLB for AOA localization while considering the flat-top antenna radiation pattern and Nakagami fading. We provided numerical

results to validate the analytical derivation and investigated the impact of various network parameters, *e.g.*, network load, path-loss, fading parameters, number of BSs, number of antenna elements, on the localization performance. The analytical framework developed in this paper offers an accurate tool to evaluate the localization performance of mmWave wireless networks, without relying on numerical simulation. The network operators can use the asymptotic bounds to optimize the network parameters and find the best deployment of the BSs to ensure the localization performance. In our future work, we will apply the approximation method to evaluate the performances of TOA, TDOA and RSS based localization and investigate the impact of various channel models.

REFERENCES

- [1] F. Khelifi, A. Bradai, A. Benslimane, P. Rawat, M. Atri, "A Survey of Localization Systems in Internet of Things", *Mobile Network and Application*, pp761–785, 2019.
- [2] W. Roh, J. Seol, J. Park, B. Lee, J. Lee, Y. Kim, J. Cho, K. Cheun, F. Aryanfar, "Millimeter-wave beamforming as an enabling technology for 5G cellular communications: Theoretical feasibility and prototype results," *IEEE Communications Magazine*, vol. 52, no. 2, pp. 106-113, Feb. 2014.
- [3] A. Alkhateeb, S. Alex, P. Varkey, Y. Li, Q. Qu and D. Tujkovic, "Deep Learning Coordinated Beamforming for Highly-Mobile Millimeter Wave Systems," *IEEE Access*, vol. 6, pp. 37328-37348, 2018.
- [4] H. C. So, "Source localization: algorithms and analysis", *Handbook of Position Location: Theory, Practice and Advances*, Chapter 3, S.A.Zekavat and M.Buehrer, Eds., Wiley-IEEE Press, 2019.
- [5] M. Haenggi, "Stochastic Geometry for Wireless Networks," Cambridge, U.K.: Cambridge Univ. Press, 2013.
- [6] Y. J. Chun, S. L. Cotton, H. S. Dhillon, F. J. Lopez-Martinez, J. F. Paris and S. K. Yoo, "A Comprehensive Analysis of 5G Heterogeneous Cellular Systems Operating Over κ - μ Shadowed Fading Channels," in *IEEE Transactions on Wireless Communications*, vol. 16, no. 11, pp. 6995-7010, Nov. 2017.
- [7] J. Schloemann, H. S. Dhillon and R. M. Buehrer, "Toward a Tractable Analysis of Localization Fundamentals in Cellular Networks," *IEEE Transactions on Wireless Communications*, vol. 15, no. 3, pp. 1768-1782, March. 2016.
- [8] C. E. O'Lone, H. S. Dhillon and R. M. Buehrer, "A Statistical Characterization of Localization Performance in Wireless Networks," *IEEE Transactions on Wireless Communications*, vol. 17, no. 9, pp. 5841-5856, Sept. 2018.
- [9] J. Khalife, C. Sevinç and Z. M. Kassas, "Performance Evaluation of TOA Positioning in Asynchronous Cellular Networks Using Stochastic Geometry Models," *IEEE Wireless Communications Letters*, May. 2020.
- [10] H. Elsawy, W. Dai, M. Alouini and M. Z. Win, "Base Station Ordering for Emergency Call Localization in Ultra-Dense Cellular Networks," *IEEE Access*, vol. 6, pp. 301-315, 2018.
- [11] K. Radnosrati, G. Hendeby, C. Fritsche, F. Gunnarsson and F. Gustafsson, "Performance of OTDOA positioning in narrowband IoT systems," in *2017 IEEE 28th Annual International Symposium on Personal, Indoor, and Mobile Radio Communications (PIMRC)*, Montreal, Canada, pp. 1-7, 2017.
- [12] J. He and H. C. So, "A Hybrid TDOA-Fingerprinting-Based Localization System for LTE Network," in *IEEE Sensors Journal*, vol. 20, no. 22, pp. 13653-13665, Nov. 2020.
- [13] A. Pin, R. Rinaldo, A. Tonello, C. Marshall, M. Driusso, A. Bionon, "LTE ranging measurement using uplink opportunistic signals and the SAGE algorithm," in *2019 27th European Signal Processing Conference (EUSIPCO)*, A Coruna, Spain, pp. 1-5, 2019.
- [14] L. Ma, N. Jin, Y. Cui and Y. Xu, "LTE user equipment RSRP difference elimination method using multidimensional scaling for LTE fingerprint-based positioning system," in *2017 IEEE International Conference on Communications (ICC)*, Paris, France, pp. 1-6, 2017.
- [15] G. Çelik, H. Çelebi and G. Tuna, "A novel RSRP-based E-CID positioning for LTE networks," in *2017 13th International Wireless Communications and Mobile Computing Conference (IWCMC)*, Valencia, Spain pp. 1689-1692, 2017.

- [16] F. Lemic, J. Martin, C. Yarp, D. Chan, V. Handziski, R. Brodersen, G. Fettweis, A. Wolisz, J. Wawrzyniak, "Localization as a feature of mmWave communication," *2016 International Wireless Communications and Mobile Computing Conference (IWCMC)*, Paphos, 2016, pp. 1033-1038.
- [17] K. Pahlavan, "Indoor geolocation science and technology," *Communications Magazine, IEEE*, vol. 40, no. 2, pp. 112-118, 2002.
- [18] F. Wen, H. Wymeersch, B. Peng, W. P. Tay, H. C. So, and D. Yang, "A survey on 5G massive MIMO localization," *Digit. Signal Process.*, 2019.
- [19] H. Wang, C. Wang, T. Zheng and T. Q. S. Quek, "Impact of Artificial Noise on Cellular Networks: A Stochastic Geometry Approach," in *IEEE Transactions on Wireless Communications*, vol. 15, no. 11, pp. 7390-7404, Nov. 2016.
- [20] B. Huang, T. Li, B. D. O. Anderson and C. Yu, "On the performance limit of sensor localization," *2011 50th IEEE Conference on Decision and Control and European Control Conference*, Orlando, FL, 2011, pp. 7870-7875.
- [21] D. Moltchanov, "Distance distributions in random networks," *Ad Hoc Networks*, vol. 10, no. 6, pp. 1146-1166, Aug. 2012.
- [22] S. Srinivasa and M. Haenggi, "Distance distributions in finite uniformly random networks: Theory and applications," *IEEE Trans. on Vehicular Technology*, vol. 59, no. 2, pp. 940-949, 2010.
- [23] M. R. Akdeniz, Y. Liu, M. K. Samimi, S. Sun, S. Rangan, T. S. Rappaport, E. Erkip, "Millimeter Wave Channel Modeling and Cellular Capacity Evaluation," *IEEE Journal on Selected Areas in Communications*, vol. 32, no. 6, pp. 1164-1179, June. 2014.
- [24] G. Lee, Y. Sung and J. Seo, "Randomly-Directional Beamforming in Millimeter-Wave Multiuser MISO Downlink," *IEEE Transactions on Wireless Communications*, vol. 15, no. 2, pp. 1086-1100, Feb. 2016.
- [25] G. Lee, Y. Sung and M. Kountouris, "On the Performance of Random Beamforming in Sparse Millimeter Wave Channels," *IEEE Journal of Selected Topics in Signal Processing*, vol. 10, no. 3, pp. 560-575, April. 2016.
- [26] Y. Wu and C. Han, "Interference and Coverage Analysis for Indoor Terahertz Wireless Local Area Networks," *2019 IEEE Globecom Workshops (GC Wkshps)*, Waikoloa, HI, USA, 2019, pp. 1-6.
- [27] J. G. Andrews, F. Baccelli, and R. K. Ganti, "A tractable approach to coverage and rate in cellular networks," *IEEE Transactions on Wireless Communications*, vol. 59, no. 11, pp. 3122-3134, Nov. 2011.
- [28] D. Zwillinger, *Table of Integrals, Series, and Products*. Amsterdam, The Netherlands: Elsevier, 2014.
- [29] M. Giordani, M. Mezzavilla, A. Dhananjay, S. Rangan and M. Zorzi, "Channel Dynamics and SNR Tracking in Millimeter Wave Cellular Systems," *22th European Wireless Conference*, Oulu, Finland, 2016, pp. 1-8.
- [30] R. Koirala, B. Denis, D. Dardari and B. Uguen, "Localization bound based beamforming optimization for multicarrier mmWave MIMO," *2017 14th Workshop on Positioning, Navigation and Communications (WPNC)*, Bremen, 2017, pp. 1-6.
- [31] D. B. Jourdan, D. Dardari, and M. Z. Win, "Position error bound for UWB localization in dense cluttered environments," in *Proc. IEEE Int. Conf. Commun.*, Istanbul, Turkey, Jun. 2006, pp. 3705-3710.
- [32] T. M. Cover and J. A. Thomas, *Elements of Information Theory*. New York, NY, USA: Wiley, 1991, chapter. 2-9.
- [33] J. Schloemann, H. S. Dhillon and R. M. Buehrer, "A Tractable Metric for Evaluating Base Station Geometries in Cellular Network Localization," in *IEEE Wireless Communications Letters*, vol. 5, no. 2, pp. 140-143, April 2016.
- [34] H. A. David and H. N. Nagaraja, *Order Statistics*. Hoboken, NJ: John Wiley and Sons, Inc., 3rd ed. 2003.
- [35] H. Elshaer, M. N. Kulkarni, F. Boccardi, J. G. Andrews and M. Dohler, "Downlink and Uplink Cell Association With Traditional Macrocells and Millimeter Wave Small Cells," in *IEEE Transactions on Wireless Communications*, vol. 15, no. 9, pp. 6244-6258, Sept. 2016.
- [36] D. B. Jourdan and N. Roy, "Optimal sensor placement for agent localization," in *Proc. IEEE/ION Position, Location, Navigat. Symp.*, Coronado, CA, USA, Apr. 2006, pp. 128-139.
- [37] C. Chang and A. Sahai, "Estimation bounds for localization," in *Proc. 1st Annu. IEEE Commun. Soc. Conf. Sensor Ad Hoc Commun. Netw.*, Santa Clara, CA, USA, Oct. 2004, pp. 415-424.